University of Baghdad
College of Engineering
JE
JOURNAL OF ENGINEERING

Journal of Engineering
journal homepage: www.joe.uobaghdad.edu.iq
Number 5 Volume 26 May 2020

***Mechanical and Energy Engineering***

# Numerical investigation on heat transfer enhancement and turbulent flow characteristics in a high aspect ratio rectangular duct roughened by intersecting ribs with inclined ribs

**Ali H. F. Theeb***
Mechanical Engineering Department,
University of Baghdad
Baghdad, Iraq
ali94.theeb@gmail.com

**Munther Abdullah Mussa**
Mechanical Engineering Department,
University of Baghdad
Baghdad, Iraq
munther@coeng.uobaghdad.edu.iq

## ABSTRACT

In this study, the effect of intersecting ribs with inclined ribs on the heat transfer and flow characteristics of a high aspect ratio duct has been numerically investigated. The Relative roughness pitch (P/e) is 10 and the Reynolds number range from 35,700 to 72,800. ANSYS (Fluent-Workbench 18.0) software has been utilized to solve the Reynolds averaged Navier-Stokes (RANS) equations with the Standard k-ε turbulence model. Three ribbed models have been used in this study. Model 1 which is a just inclined ribs, Model 2 which has a single longitudinal rib at the center with inclined ribs and Model 3 which has two longitudinal ribs at the sides. The results showed that the heat transfer rate has been enhanced when the intersecting ribs are used. Model 3 has achieved the highest overall thermal performance. The increasing in Nusselt number ratio ($Nu / Nu_s$) for Model 3 and 2, relative to Model 1, are 13.19% and 7.03%, respectively. Consequently, the hybridizing by intersecting ribs with inclined ribs is considered as an advantageous technique to enhance the heat transfer.

**Keywords:** Heat transfer, Intersecting ribs, Vortices, Overall thermal performance, CFD

# دراسة عددية حول تحسين أنتقال الحرارة وخصائص التدفق المضطرب في قناة مستطيلة ذات نسبة عالية للجوانب مخشنة بواسطة حزوز متقاطعة مع حزوز مائلة

**منذر عبدالله موسى**
قسم الهندسة الميكانيكية
جامعة بغداد

***علي حسين فاضل ذيب**
قسم الهندسة الميكانيكية
جامعة بغداد

## الخلاصة

في هذا العمل الحالي, تم أجراء دراسة نظرية في خصائص انتقال الحرارة والجريان لتأثير الحزوز المتقاطعة مع الحزوز المائلة من خلال مجرى هوائي ذو نسبة العرض إلى الارتفاع كبيرة. وكانت نسبة المسافة بين الحزين الى أرتفاع الحز تساوي 10 ونسبة أرتفاع الحز الى القطر الهيدروليكي تساوي 0.068. وقد أستخدم برنامج ANSYS (Fluent-Workbench

*Corresponding author
Peer review under the responsibility of University of Baghdad.
https://doi.org/10.31026/j.eng.2020.05.02

Article received: 2 /4//2019
Article accepted: 2/6/2019
Article published:1/5/2020

(18.0 في حل معادلات ال(RANS) بأستخدام نموذج الاضطراب( Standard k-ε). وقد أدى أستخدام الحزوز المتقاطعة الى توليد دوامات جديدة في كل نقطة تقاطع أضافة الى الدوامات الاولية المتولدة في الجهة الرئيسية للحزوز المائلة. لذا فان انتقال الحرارة في الجهة الخلفية للحزوز المائلة قد تحسن. وبالتالي تم تحسين الاداء الحراري الكلي. وقد تم أستخدام ثلاث نماذج مخشنة لدراسة هذه الحالة. النموذج 1 عبارة عن حزوز مائلة تمامًا ، أما النموذج 2 فيحتوي على حز طوليً واحدً في الوسط مع الحزوز المائلة ، أما النموذج الثالث فيحتوي على حزين طوليين على الجانبين. أظهرت النتائج ان معدل انتقال الحرارة قد تحسن عند أستخدام الحزوز المتقاطعة. وقد أظهر النموذج 3 أعلى القيم في الأداء الحراري الكلي. لذلك ,فأن التهجين بأستخدام الحزوز المتقاطعة مع الحزوز المائلة يعتبر تقنية مجدية لتحسين أنتقال الحرارة.

**الكلمات الرئيسية:** انتقال حرارة, حزوز متقاطعة , دوامات, الاداء الحراري الكلي, ديناميكا الموائع الحسابية.

## 1. INTRODUCTION

Many of thermal systems require an enhancement in the heat transfer rates for saving power exhaustion. Different mechanisms for enhancing thermal performance have been used. The suitable type of heat transfer enhancement technique can be selected according to the required level of augmentation, geometry, pressure drop and the cost. The artificial surface roughness in the form of ribs has been suggested to use. This type may be used in several engineering applications, such as solar air heater and gas turbines.

**(Lee et al., 2009)** investigated the flow characteristics and local heat/mass transfer on the effect of aspect ratio (AR) for ribbed duct for two different V-shaped rib configurations. They were observed that the heat/mass transfer at the center zone of channel was significantly affected by the (AR), since heat/mass transfer rate decreased as the (AR) increased. Also, pressure drop increased with increasing the (AR).

**(Aliaga et al., 1994)** experimentally observed that a separation-reattachment flow phenomenon occurred at P/e = 12 and a single vortex flow enclosed between ribs at p/e = 5. They discussed the heat transfer distribution, therefor, they found that best heat transfer coefficient on the middle of top surface of the rib occurred at P/e = 12 and at the upstream corner. (**Taslim and Liu, 2005)** experimentally and numerically showed that the 45◦ inclined ribs with (e/Dh >0.2) at high Re had law thermal performance. They observed that the CFD simulation can be considered is a good way to prediction heat transfer fields for ribbed surface. **(Lu and Jiang, 2006)** experimentally and numerically investigated the effect of mass flow rate on the heat transfer and flow characteristics for inclined ribs in a rectangular duct. The CFD FLUENT 6.1 with SST k– ω turbulence model used to get numerical results and showed a good acceptability with experimental part. The results showed that the heat transfer coefficients increase with increasing the flow rate and decreasing with reduced the spacings. The angle of 60° achieve highest heat transfer coefficients. **(Aharwal et al., 2008)** experimentally studied the effect of gaps with the inclined ribs in a rectangular duct on the characteristics of flow heat transfer. Specially, reported the influence of the width and the position for gap at Re range from $3x10^3$ to 18 $x10^3$. The experiments were performed with (AR =1: 5.84) roughened by inclined rib at $60^o$ angle of attack with and without a gap. It was observed that the gap has significantly effect on the heat transfer and flow characteristics. However, the maximum increasing in Nusselt number and friction factor were 2.59 and 2.87 times with respect to the smooth duct, respectively. Also, the best overall thermal efficiency was found at the relative gap position of 0.25 and the relative gap width of 1. **(Alkhamis et al., 2011)** experimentally found that both the friction factors and heat transfer coefficients increase when increase the rib height (e) or the rib to rib spacing (p), because of the increasing in flow turbulence. The V-shaped ribs showed good performance in heat transfer enhancement with a little pressure drop. Also, observed that the efficiency indices decreased below one at higher Reynolds number. **(Chung et al., 2015)** experimentally and numerically investigated the intersecting rib effect with inclined ribs at $60^o$ attack angle on heat/mass transfer efficiency. They used a rectangular duct with different aspect ratio (W/H) was varied from 1 to 4. They observed an enhancement in locally heat/mass transfer performance, especially for aspect ratio (W/H = 2.0) that shows optimum performance. Also, they suggested to use more than an intersecting rib with a high aspect ratio channel. **(Kim et al., 2016)** numerically showed that the shape and location of recirculation and reattachment regions were changed due to the different inlet velocity profiles. Also, they conclude that the profile of fully

developed flow was showed the best thermal efficiency, that because of induced a little pressure drop. **(Ravi et al., 2017)** numerically studied the effect of rib geometries; V- formed, W- formed, $45^{o}$ inclined and M- formed ribs in a two-pass square duct on characteristics of flow and heat transfer. Software ANSYS Fluent utilized to solve the Reynolds averaged Navier Stokes equations by using RNG k-ε turbulence model. It was found that the flow and heat transfer the in the second passage effected by vortices that induced in the bend. V- formed ribs had been offered the maximum enhancement in overall heat transfer at the first and second passage. **(Yang et al., 2017)** experimentally and numerically studied the characteristics of flow and heat transfer rate for a square ribbed duct by ribs with high blockage ratio (e/H) in opposite form. FLUENT-6.3 was utilized for numerical work by used k-ε turbulence model to simulate flow and heat transfer fields. The rib configuration had been showed an important effect on the heat transfer rate of roughened ducts. Generally, the average Nusselt number of staggered ribs is less than that of symmetric ribs. Of the above review, the previous researchers did not adequately cover the matter of the effect of the inclined ribs in a rectangular duct with a high aspect ratio. Moreover, there is a lack in the information available on dealing with the problem of span-wise variation of heat transfer which induced with the inclined ribs. Accordingly, the present work objective is to numerically investigate the effect of used intersecting ribs with inclined ribs in a rectangular duct of a high aspect ratio, on heat transfer and characteristics of flow. Also, to determine the optimum model that achieves the highest heat transfer enhancement with the lower pressure drop ز

## 2. MODELLING AND CFD SIMULATION

### 2.1 Computational Condition

The geometry of present study is a rectangular duct with rib-roughened surface by angled and intersecting ribs. The geometry adopting by; firstly, modeling the aluminum test plate of 500 mm × 400 mm × 5 mm, creating smooth surface then set the ribs over the plate. Forming the duct as a box and specifying the domain as fluid and the test plate as solid, as shown in **Fig.1**, that clarify the test section. The geometry is divided into three sections; inlet section, test section and exit section. The cross section of the duct is 400 mm×40 mm with an aspect ratio (AR=10). The ribs are also aluminum with square cross section of 5 mm × 5 mm and utilized in different arrangement for three models. Model (1) is the surface roughened by the angled ribs with 75° attack angle. While, Model (2) the surface is roughened by an inclined rib with an intersecting rib at the center of the plate parallel to the main flow.

Model 3 is somewhat look like Model 2 but it different by added two intersecting ribs at the sides instead of one at the center, as shown in **Fig. 2**. Reynolds number range of 35,700 to 72,800, rib

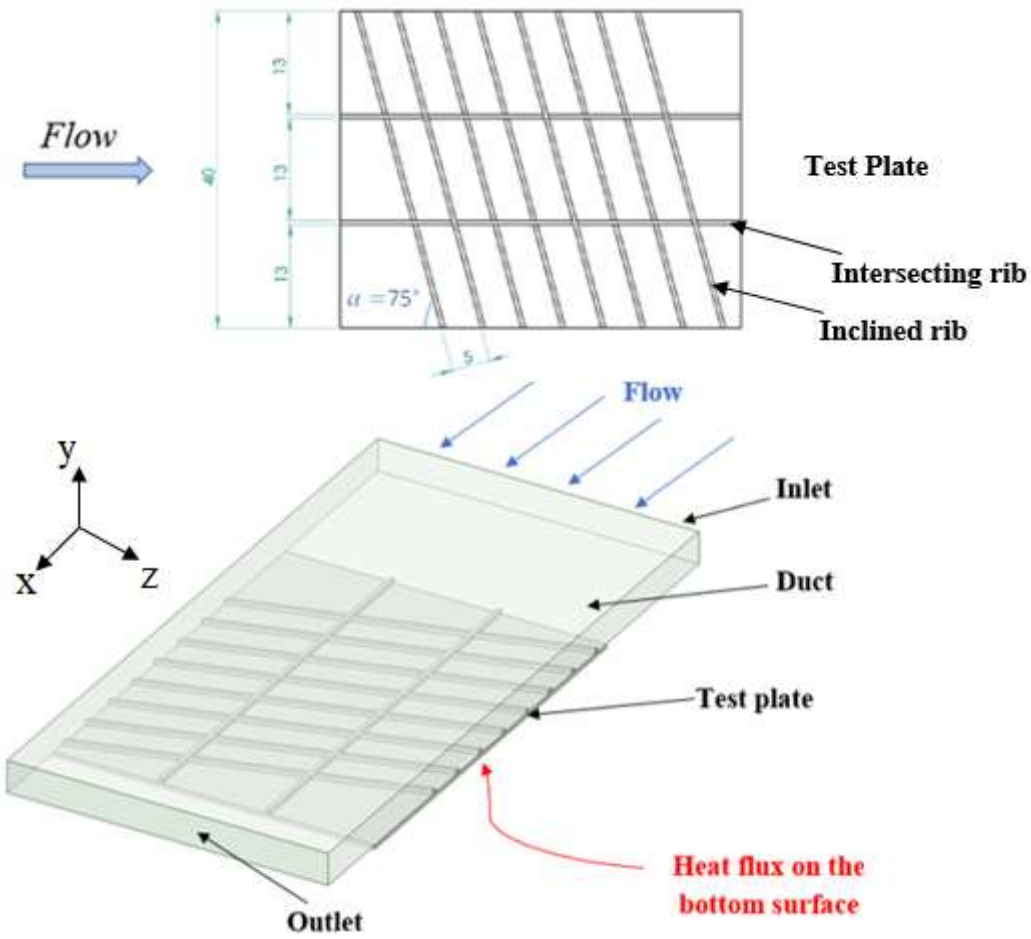


pitch (P) of 50 mm and rib height (e) of 5 mm. Since,

**Figure 1**. Domain of computation and modeled view for test section. (Unit in cm)

relative roughness pitch (p/e) and relative roughness height ($e/D_h$) of 10 and 0.068, respectively.

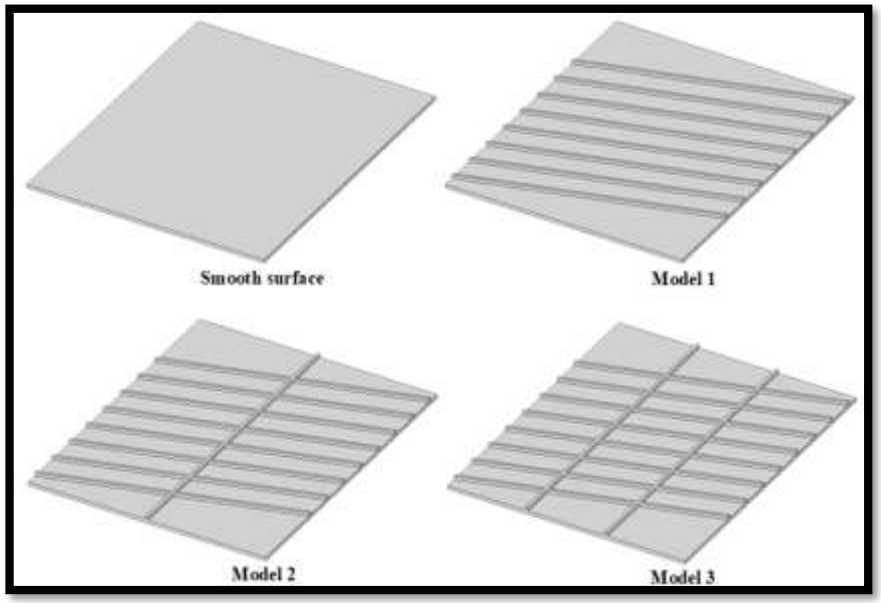


**Figure 2**. Test plates.

## 2.2 Mesh Generation

unstructured tetrahedral grids are generated for the domain. For mesh independence test, four mesh numbers of Model 2 had been tested in the independence study, with 1.3, 2.1, 2.8 and 3.6 million elements, respectively. For all the used mesh numbers, the obtained averaged Nusselt number exhibit teeny differences between the finest and coarsest mesh, was observed around 4%, as shown in **Fig. 3**. Considering both the solution precision and calculation efficiency, the mesh number of 2.8 million was adopted in the present study and depends on the different computational ribbed models. To get good quality, the cells of mesh structure should be fine in all domain. Therefore, the mesh should be adjusted manually in some regions to ensure smooth and accurate mesh for a three-dimensional model, as shown in **Fig. 4**. A size function was applied for all geometry at minimum size of 1 mm, maximum size of 3mm and growth rate of 1.10, with an average skewness of cells 0.23.

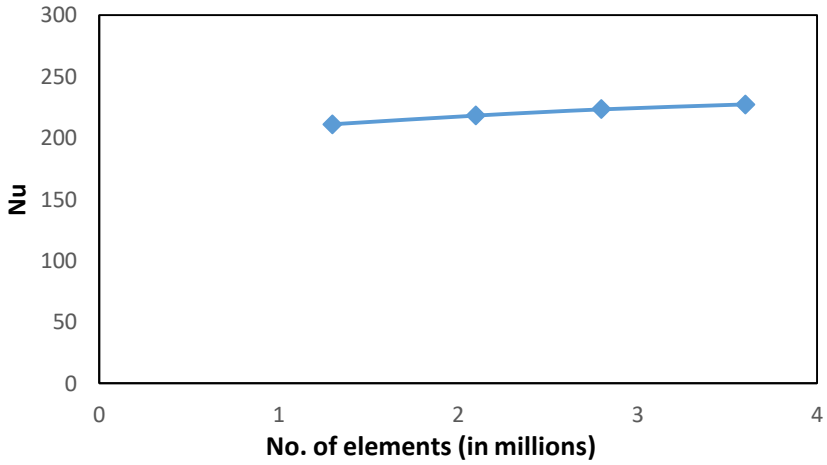


**Figure 3**. Overall average Nusselt number enhancement for different grid system.

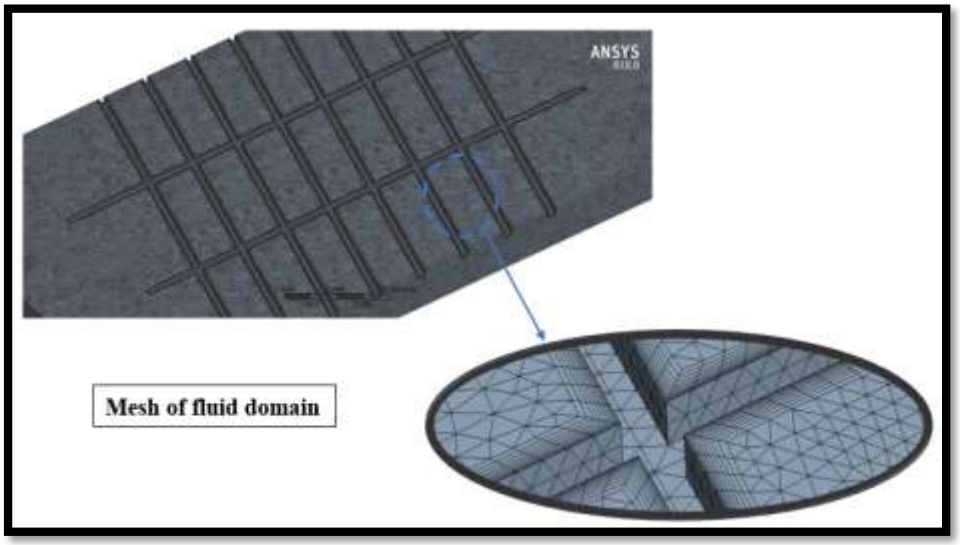


**Figure 4**. Structured grid employed for computations.

### 2.3 Governing Equation

In case of turbulent flow in rectangular coordinates, the governing equations of continuity, energy and momentum were utilized to study the motion of particles inside the fluid domain. Which defines the heat transfer and flow characteristics. The several assumptions which had been considered in the analysis are:

- Steady state, incompressible and three-dimensional flow with constant fluid properties.
- The heat flux is uniform at the plate surface.
- No-slip wall boundary condition.
- Radiation heat transfer is negligible.
- No buoyancy effect ($G_b = 0$).

Based on the above assumptions, the Reynolds Averaged Navier-Stokes Equations (RANS) are mostly used to characterize turbulent flows, (**Jones and Clarke, 2005),** can be written as:

Continuity Equation:

$$\frac{\partial}{\partial x_i}(\boldsymbol{\rho u_i}) = \mathbf{0} \tag{1}$$

Momentum Equation:

$$\frac{\partial}{\partial x_i}\left(\overline{\boldsymbol{\rho u_\iota u_j}}\right) = -\frac{\partial \bar{P}}{\partial x_i} + \frac{\partial}{\partial x_i}\left[\boldsymbol{\mu}\left(\frac{\partial \bar{u}_i}{\partial x_j} + \frac{\partial \bar{u}_j}{\partial x_i} - \frac{2}{3}\boldsymbol{\delta_{ij}}\frac{\partial \bar{u}_i}{\partial x_j}\right)\right] + \frac{\partial}{\partial x_i}\left(-\overline{\boldsymbol{\rho u_\iota' u_j'}}\right) \tag{2}$$

Energy Equation:

$$\frac{\partial}{\partial x_i}[\boldsymbol{u_i}(\boldsymbol{\rho E} + \boldsymbol{p})] = \frac{\partial}{\partial x_i}\left[\left(\boldsymbol{k} + \frac{\boldsymbol{\mu_t C_p}}{\boldsymbol{Pr_t}}\right)\frac{\partial \boldsymbol{T}}{\partial x_i} + \boldsymbol{u_i}(\boldsymbol{\tau_{ij}})_{\boldsymbol{eff}}\right] \tag{3}$$

Where:

$$\boldsymbol{E} = \boldsymbol{C_p T} - \frac{\boldsymbol{P}}{\boldsymbol{\rho}} + \frac{\mathbf{1}}{\mathbf{2}}(\boldsymbol{u^2} + \boldsymbol{v^2} + \boldsymbol{w^2}) \tag{4}$$

$$(\boldsymbol{\tau_{ij}})_{\boldsymbol{eff}} = \boldsymbol{\mu_{eff}}\left[\left(\frac{\partial u_i}{\partial x_j} + \frac{\partial u_j}{\partial x_i}\right) - \frac{2}{3}\boldsymbol{\delta_{ij}}\frac{\partial u_i}{\partial x_j}\right] \tag{5}$$

$$\boldsymbol{\mu_{eff}} = \boldsymbol{\mu} + \boldsymbol{\mu_t} \tag{6}$$

### 2.4 Data Reduction

The temperature of the top surface for test plate ($T_s$) and the air bulk temperature ($T_b$), used to estimate the heat transfer coefficient (h) as (**Alfarawi et al., 2017**):

$$h = \frac{q_{conv.}}{(T_s - T_b)} \tag{7}$$

where the ($q_{conv.}$) is equal to the heat flux value that applied on the bottom surface of the test plate, with no losses. The Nusselt number and Reynolds number were estimated by **(Aharwal et al., 2008), (Ezzat and Ghashim, 2019)**:

$$Nu = \frac{h\, D_h}{K_{air}} \tag{8}$$

$$Re = \frac{u_m\, D_h}{\nu} \tag{9}$$

Where $D_h$ is the hydraulic diameter was estimated as (**Alfarawi et al., 2017), (Mahdi and Gaddoa, 2019)**:

$$D_h = \frac{4(W*H)}{2(W+H)} \quad (10)$$

The friction factor (f) was evaluated as **(Yang et al., 2017)**:

$$f = \left(\frac{\Delta P}{2\,\rho u_m^2}\right)\left(\frac{D_h}{L}\right) \quad (11)$$

where ΔP is the pressure drop along the test section, L is the length of the test section, $\rho$ is the air density and the $u_m$ is the mean velocity. The air properties were estimated at the mean temperature of flow ($T_f$):

$$T_f = \frac{(T_{in}+T_{out})}{2} \quad (12)$$

Where, $T_{in}$ is the inlet air temperature at 5 cm from the inlet of test Plate and $T_{out}$ is the outlet air temperature at 5 cm from the end of test section. Nusselt number ratio, friction factor ratio and overall thermal performance ($\eta$)are defined as (**Alfarawi et al., 2017**):

Nusselt number ratio = $(Nu / Nu_s)$ (13)

Friction factor ratio = $(f/f_s)$ (14)

Where $Nu_s$ and $f_s$ are Nusselt number and Friction factor for the smooth surface.

### 2.5 Boundary Condition & Fluid Flow Turbulence Model

To solve the equations and simulate the heat transfer and fluid flow over the ribbed plate in rectangular channel, the domain is separated as; inlet, pressure outlet, wall and Symmetric boundaries. Uniform velocity of air and temperature was specified as the inlet boundary conditions. For all cases, the velocity at the inlet was (7.7, 9.7, 11.7, 13.7, 15.7) m/s with a constant heat flux of 1000 W/m$^2$ was imposed on the bottom wall and ribs. There are several turbulence models which utilized to study the heat transfer and flow fields. Generally, The Standard k-ε turbulence model is currently the most widely utilized turbulence model in simulation of engineering flows as it provides acceptable accuracy for a wide range of turbulence flows. In addition to that, it is widely used in heat transfer simulation, as observed in some literature studied (**Ravi et al., 2017)**, (**Yang et al., 2017)** and (**Taslim et al., 2005).**

The transport equation for $k$ is physically correct, however the transport equation for ($\varepsilon$), is heavily modelled **(Mulvany et al., 2004)**. To found the turbulence kinetic energy ($k$) with its amount of dissipation ($\varepsilon$), the following transport had been used **(Fluent 17.1 User's Guide, 2018)**.

Turbulence kinetic energy ($k$)equation: -

$$\frac{\partial}{\partial x_i}(\boldsymbol{\rho k u_i}) = \frac{\partial}{\partial x_j}\left[\left(\mu + \frac{\mu_t}{\sigma_k}\right)\frac{\partial k}{\partial X_j}\right] + \boldsymbol{G_K} - \boldsymbol{\rho}\varepsilon + \boldsymbol{S_k} \quad (16)$$

The dissipation rate of turbulence energy ($\varepsilon$) equation: -

$$\frac{\partial}{\partial x_i}(\boldsymbol{\rho}\varepsilon\boldsymbol{u_i}) = \frac{\partial}{\partial x_j}\left[\left(\mu + \frac{\mu_t}{\sigma_\epsilon}\right)\frac{\partial \varepsilon}{\partial X_j}\right] + \boldsymbol{C_{1\epsilon}}\boldsymbol{G_k}\frac{\boldsymbol{\varepsilon}}{\boldsymbol{k}} - \boldsymbol{C_{2\varepsilon}}\boldsymbol{\rho}\frac{\boldsymbol{\epsilon^2}}{\boldsymbol{k}} + \boldsymbol{S}_\varepsilon \quad (17)$$

where ($G_k$) expresses the generation of turbulence kinetic energy due to the mean velocity gradients, this term may be defined as **(Fluent 17.1 User's Guide, 2018)**:

$$G_k = -\rho\overline{u_i' u_j'}\frac{\partial u_j}{\partial x_i} \quad (18)$$

where $S_k$ and $S_\varepsilon$ are user-defined source terms. And ($C_{1\epsilon}, C_{2\epsilon}, C_\mu, \sigma_k$ *and* $\sigma_\epsilon$ ) are the model constants and have the default values;

$$C_{1\epsilon} = 1.44, C_{2\epsilon} = 1.92, C_\mu = 0.09, \sigma_k = 1.0, \sigma_\epsilon = 1.3$$

## 3. VALIDATION FOR CONVECTION HEAT TRANSFER

The numerical results of heat transfer field of flow through a duct roughened by intersecting/inclined ribs for the present work is compared with the with the results by **(Chung et al., 2015)** as shown in **Fig. 5**. Apparently, the results from both works are in good agreement. For Model 1 in both cases, high heat transfer coefficient regions were observed in the leading side of inclined ribs and decreased gradually towards the trailing region. While for Model 2, the high heat transfer coefficient regions were doubled and re-appear in the intersection in addition to the leading side.

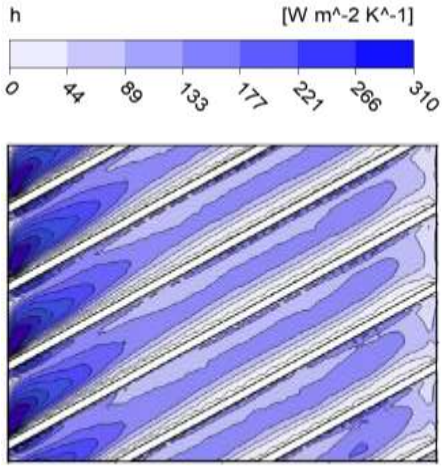


**(a) Model 1 by Chung et.al 2015**

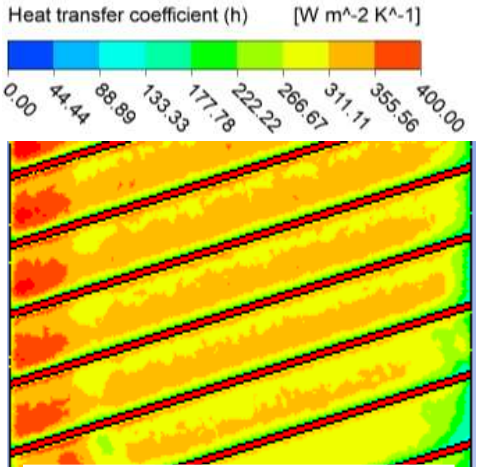


**(b) Model 1 in the present work**

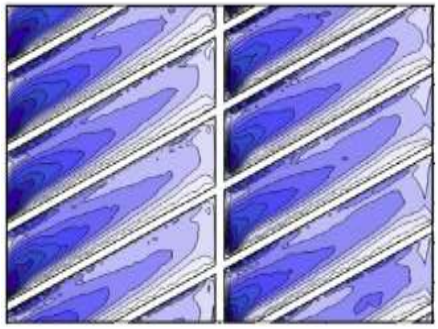

**(c) Model 2 by Chung et.al 2015**

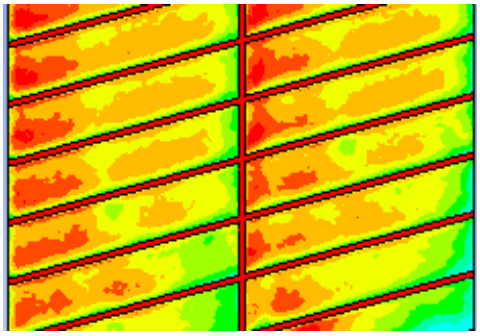

**(d) Model 2 in the present work**

**Figure 5**. Heat transfer coefficient distribution for the present work and for the researcher **Chung et.al 2015**.

## 4. RESULTS AND DISCUSSION

### 4.1 Flow Characteristics

In order to study heat transfer and characteristics of flow passing over a roughened model, it is important to understand the mechanisms of the flow and the inbred behavior of secondary flows which generated by the inclined ribs. The secondary flows are showed clearly by CFD analysis for Re=72,800 as vortices.

For Model 1 which is the inclined ribs model, **Fig. 6** shows the streamlines on three (x-y) planes along the flow direction. The vortices are induced at the leading side corner of every rib with rotating in counter-clockwise orientation, as shown in **Fig. 6**(a), and these vortices move immediately to the trailing side corner. However, due to the sloping of the ribs, a rotational motion of the fluid was induced behind the ribs, which lead to move the vortices diagonally in accordance to that motion. The strength of these vortices gradually diminished and their shape changed, during this moving from the leading side to the trailing side as shown in **Fig. 6**(b) and (c). The dissipation of the vortices is showing clearly at trailing side (**Fig. 6**(c)).

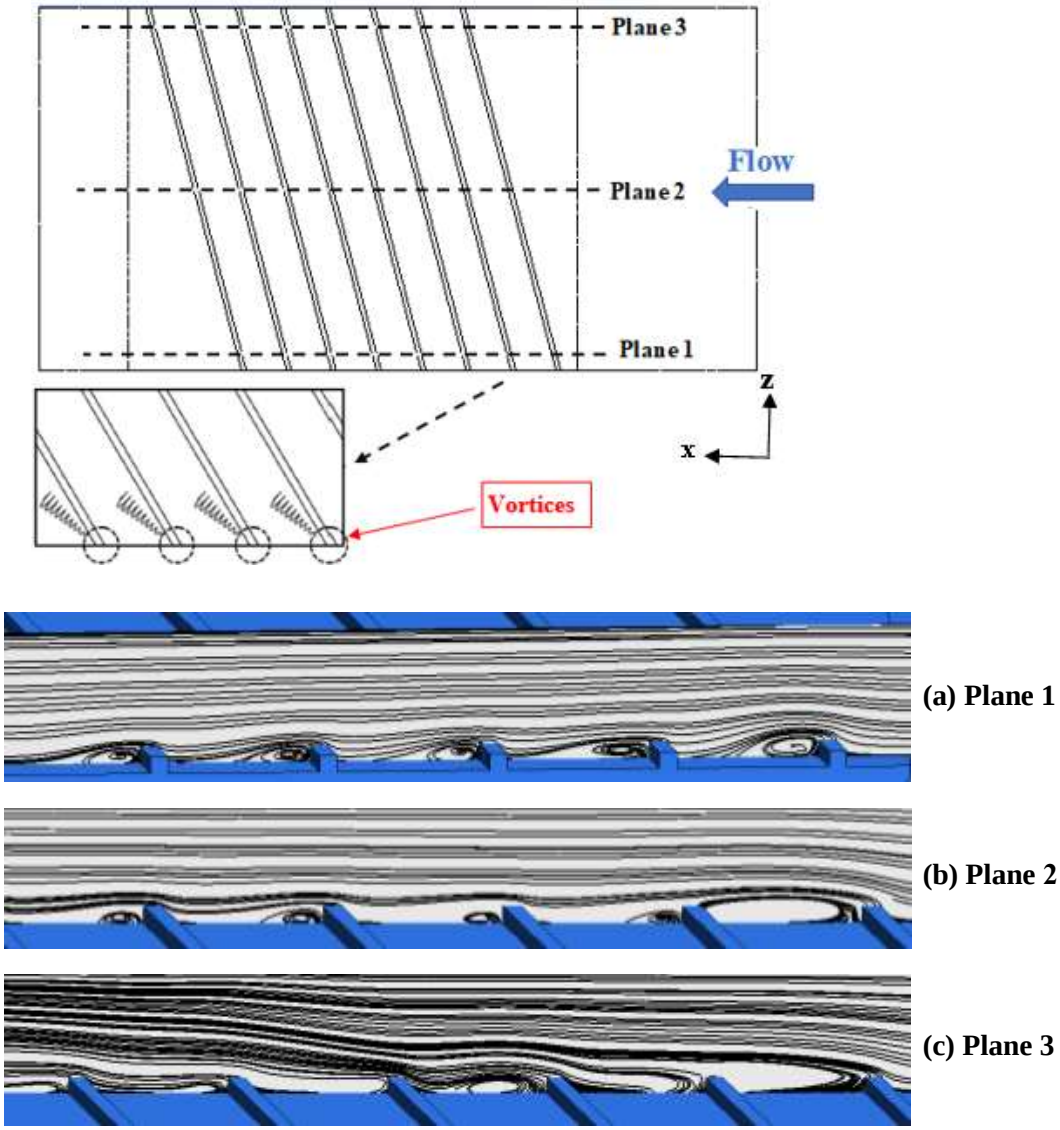


**Figure 6**. Contours of the Streamline on three x-y Planes Between the First Rib and Fifth Rib for Model 1 at Re = 72,800: a) Plane 1 at z = 2; b) Plane 2 at z = 20; c) Plane 3 at z = 38.

Accordingly, this phenomenon reduces heat convection from heated surface to air flow at the trailing region . Hence, to overcome this disadvantage, Model 2 had been suggested which is used longitudinal ribs added with parallel to the flow direction to intersect the inclined ribs.

**Fig. 7** shows the streamlines on five (x-y) planes for Model 2. With the presence of the intersecting rib, the vortices are starting from the leading side and moving behind the rib, until dissipate when reaching the intersecting rib, because of the flow is separating when it confronts the intersecting rib, as shown in **Fig. 7**(a) and (b). Then, the vortices are completely disappearing on the top of the intersecting rib, as shown in **Fig. 7**(c). After that, the vortices that induced at the leading corner of the inclined ribs are regenerated directly behind the intersecting rib, as revealed by **Fig. 7**(d), and thereafter it dissipated at the trailing corner, as observed in **Fig. 7**(e). Consequently, this behavior increased the heat transfer in the trailing region. To duplicate the regeneration of vortices, a second longitudinal rib had been added in Model 3. Therefore, the behavior that happened in the Model 2 is repeating for each intersecting rib.

**Fig. 8** shows the pressure distributions on the test surface for the three models at Re = 72,800. In general, the high-pressure regions are existed where the flow strike the ribs. The low-pressure regions happened at downstream the ribs where the vortices are induced. Obviously, the low-pressure regions concentrated intensively at the leading side for model 1, and at the intersection points for Model 2 and 3 besides the leading side. This means that the stronger vortices lead to a higher-pressure loss. The pressure loss gradually increases along the flow direction is due to the repeated ribs.

**Fig. 9** presents swirling patterns in (y-z) plane, which created in test duct with and without intersecting rib at Re = 35,700. For Model 1, one swirl is showed, which induced by the inclined rib, as shown in **Fig. 9** (a). In case of Model 2, double swirls were generated due to the dichotomy by the intersecting rib, as shown in **Fig. 9** (b). Therefore, the flow mixing and turbulence effect would be highly augmented with this effect, for this reason Model 2 provides higher heat transfer than model 1. In model 3, three swirls were observed with different locations compared to Model 2, effected by the intersecting ribs, as shown in **Fig. 9** (c). So, the flow mixing and turbulence effect would be increased, consequently, increased the heat transfer for Model 3.

### 4.2 Temperature Field

**Fig. 10** shows the temperature distribution contours of the contact-region of air with the heated surface in (x-z) plane for the three ribbed models at Re=72,800. For the case of using the inclined ribs only (Model 1), the temperature gradually increases from the leading side (P1) towards the trailing side (P2), as shown in **Fig. 10**(a). Whereas, (P1) represents the low temperature region with high convection heat transfer at **Fig. 10**, while (P2) represents the high temperature region with low convection heat transfer. This span-wise variation in the heat transfer is due to the vortices that generated in the leading corner of the ribs and moved directly behind these ribs. However, these vortices bring the cooler air firstly in contact with leading corner, and then gradually diminish in until reach the trailing corner. Therefore, a locally enhanced in heat transfer observed at leading region, while the trailing region heat transfer is relatively low.

For the case of Model 2, the temperature distribution in the leading region is similar to that of Model 1, as shown in **Fig. 10**(b). while, the number of regions with low temperature (P1) is double and appear for a second time directly behind the intersecting rib. Although, the high temperature region (P2) reduced at the trailing side, but it somewhat appeared in the adjacent of the intersecting rib because of the flow separation at the confronts of the intersecting rib

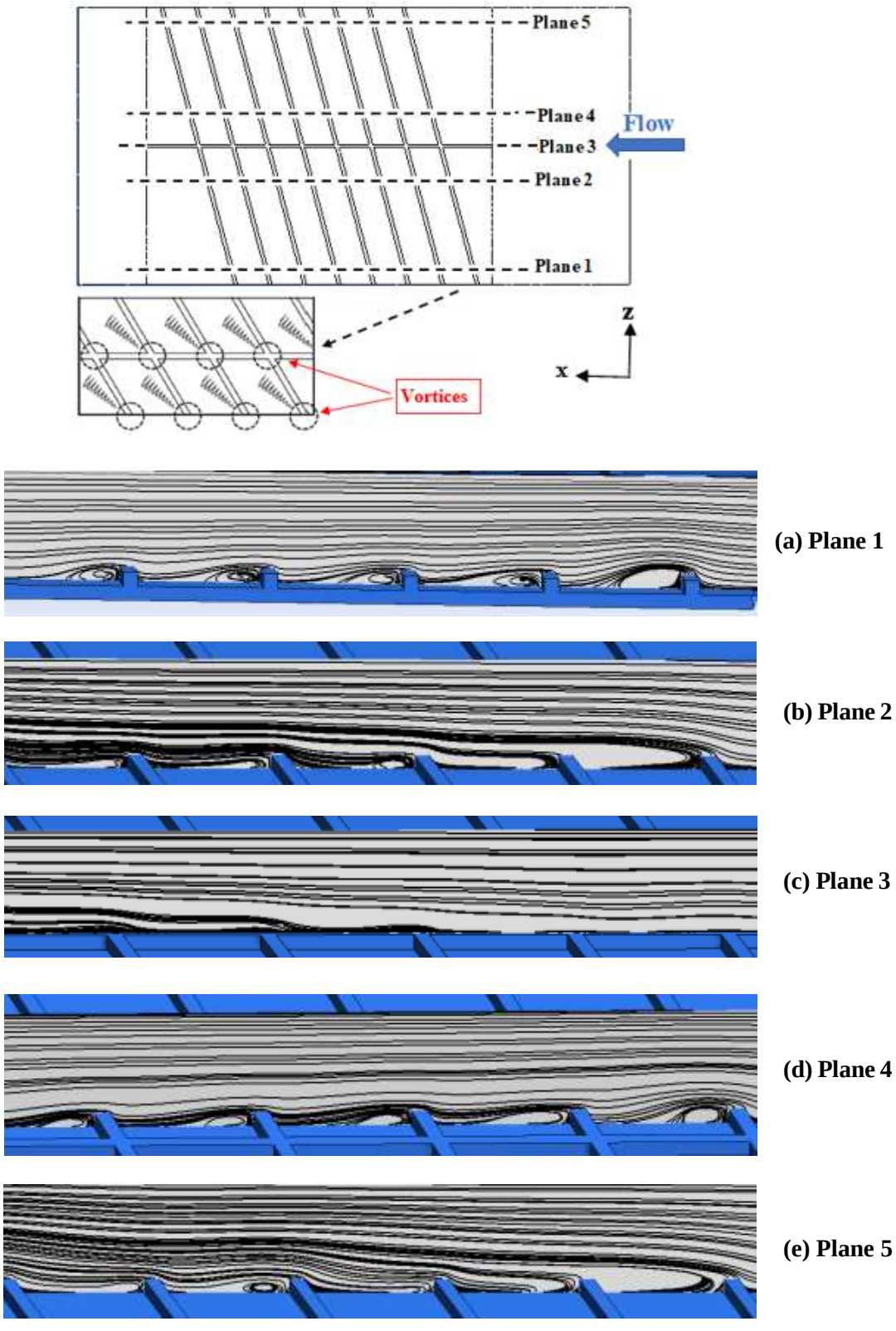


**Figure 7**. Contours of the Streamline on Five x-y Planes Between the First Rib and Fifth Rib for Model 2 at Re = 72,800: a) Plane 1 at z = 2; b) Plane 2 at z = 16; c) Plane 3 at z = 20; d) Plane 4 at z = 24; e) Plane 5 at z = 38

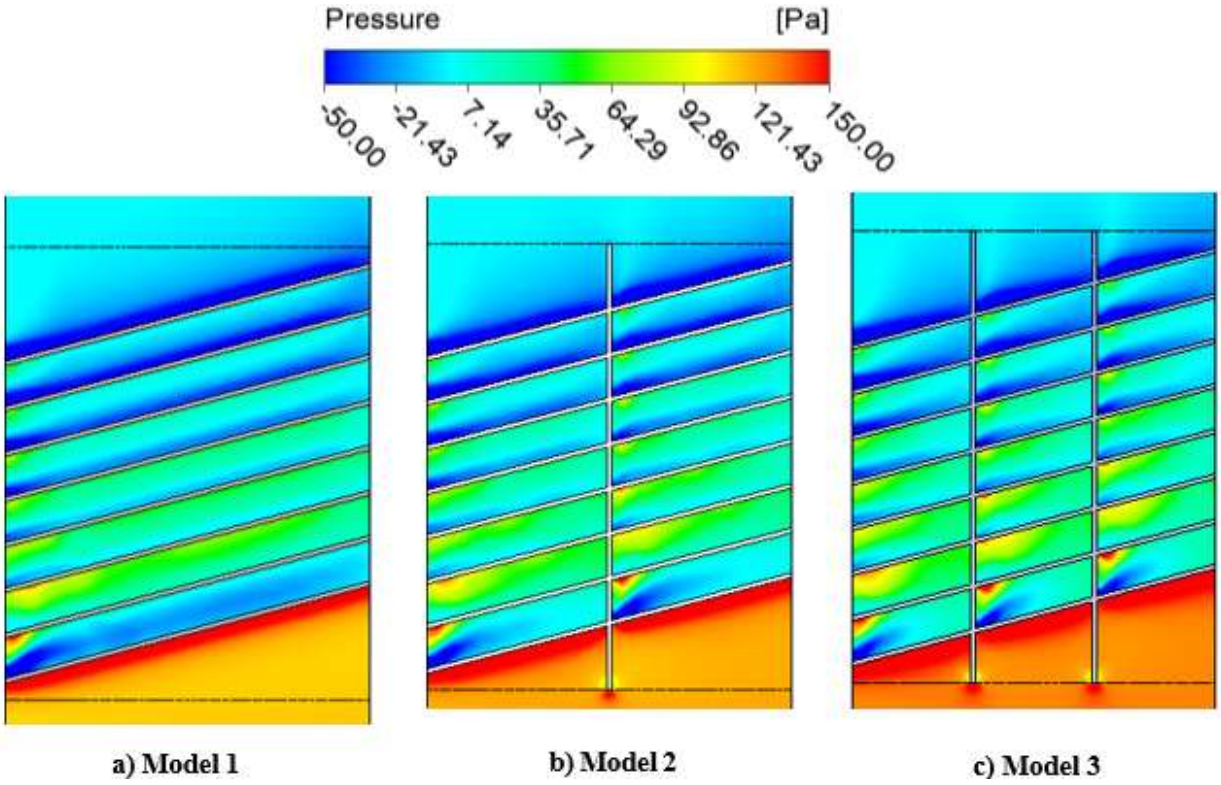


**Figure 8**. Contours of the Pressure Distributions on the Bottom Surface of Ribbed Models at Re = 72,800: a) Model 1; b) Model 2; c) Model 3.

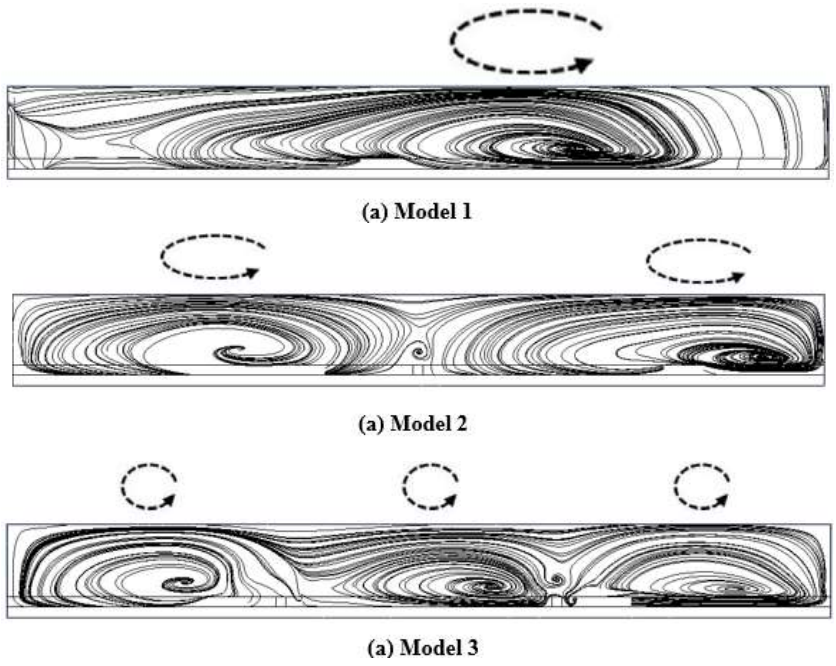


**Figure 9.** Swirling Motions on (y-z) Plane at the Center of Test Plate at Re = 35,700: a) Model 1; b) Model 2; c) Model 3

. The new region of low temperature is appearing due to the regeneration of the new vortices at the intersection point. Theses vortices increase the turbulence of the flow and lead to destroy the boundary layer between the inclined ribs. Therefore, with the intersecting rib, the enhancement of locally heat transfer is a double, and the overall heat transfer performance is improved with the interesting rib.

In order to increase the local heat transfer, two interesting ribs had been used in Model 3. According to **Fig. 10**(c), it is obvious that the low temperature (P1) is treble, and the high temperature region (P2) is almost diminishing, as a result of the regeneration vortices by the second interesting rib. So, the heat transfer is locally enhancing at three regions rather than two, Consequently, the overall heat transfer performance is clearly improving as comparison to Model2. Apparently, the low temperature regions (P1) are smaller and high temperature regions (P2) are larger with Reynolds number decreasing at (Re=54,300), as depicted in **Fig. 11** in addition to **Fig. 10**. It is a naturalist result because of the heat transfer enhancement decreases as Reynolds number decreasing.

### 4.3 Overall Thermal Performance

It had been explained above that the intersecting ribs improve the heat transfer but accompanied with higher pressure drop penalty. Therefore, it is essential to calculate the overall thermal performance to find the optimal model that achieve an enhancement in heat transfer with a minimum pressure drop penalty. (**Lewis, 1975)** presented an efficiency parameter '$\eta$' that represents the overall thermal performance, it defined as:

$$\eta = (Nu / Nu_s) / (f / f_s)^{1/3} \quad (18)$$

**Fig. 12**. shows the variation of the overall thermal performance against Reynolds Number. It can be observed that the efficiency $(\eta)$ for Model 3 is higher than those of the Model 2 and 1. This clarify that the intersecting ribs showed excellent performance with inclined ribs. Thus, the hybridizing by intersection ribs with inclined ribs is considered useful technique to enhanced the heat transfer, rather than using inclined ribs alone.

## 5. CONCLUSIONS

Based on the numerical investigation of heat transfer and flow characteristics of turbulent flow in a rectangular duct roughened by intersecting ribs with inclined ribs, the following conclusions have been recorded:

- The enhancement in the heat transfer by the intersecting ribs is usually coupled with increases in the pressure drop. In spite of that, the overall thermal performance can be increased.
- Model 3 achieves the highest overall thermal performance compared to Model 2 and Model 1.
- The increasing in Nusselt number ratio ($Nu / Nu_s$) for Model 3 and 2, relative to Model 1, are 13.19% and 7.03%, respectively.
- The temperature gradient in the span direction (along the inclined rib) is larger than that in the flow direction.

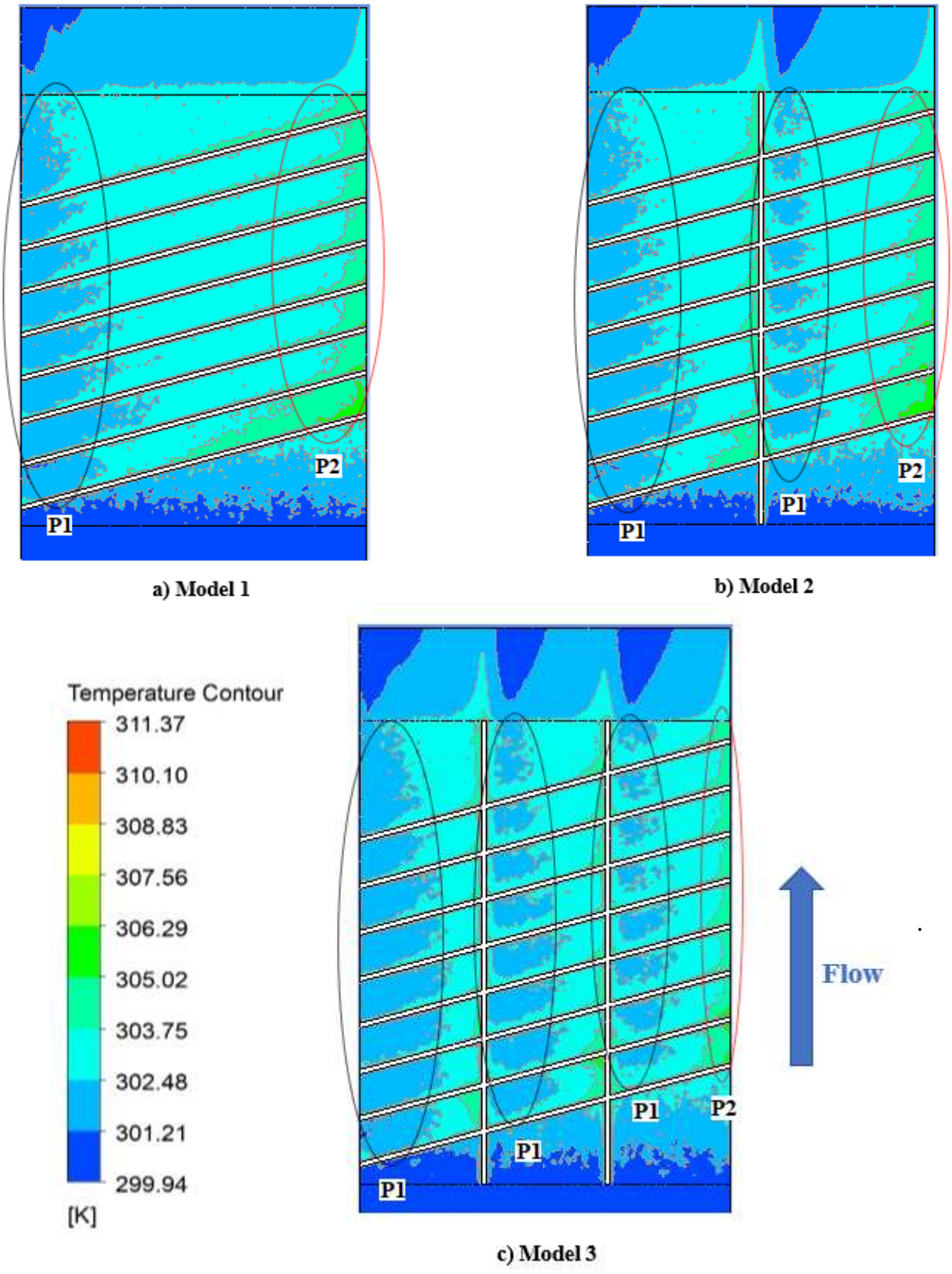


**Figure 10**. Contours of the Fluid Temperature Distribution on the Bottom Surface of Ribbed Models at Re=72,800: a) Model 1; b) Model 2; c) Model 3.

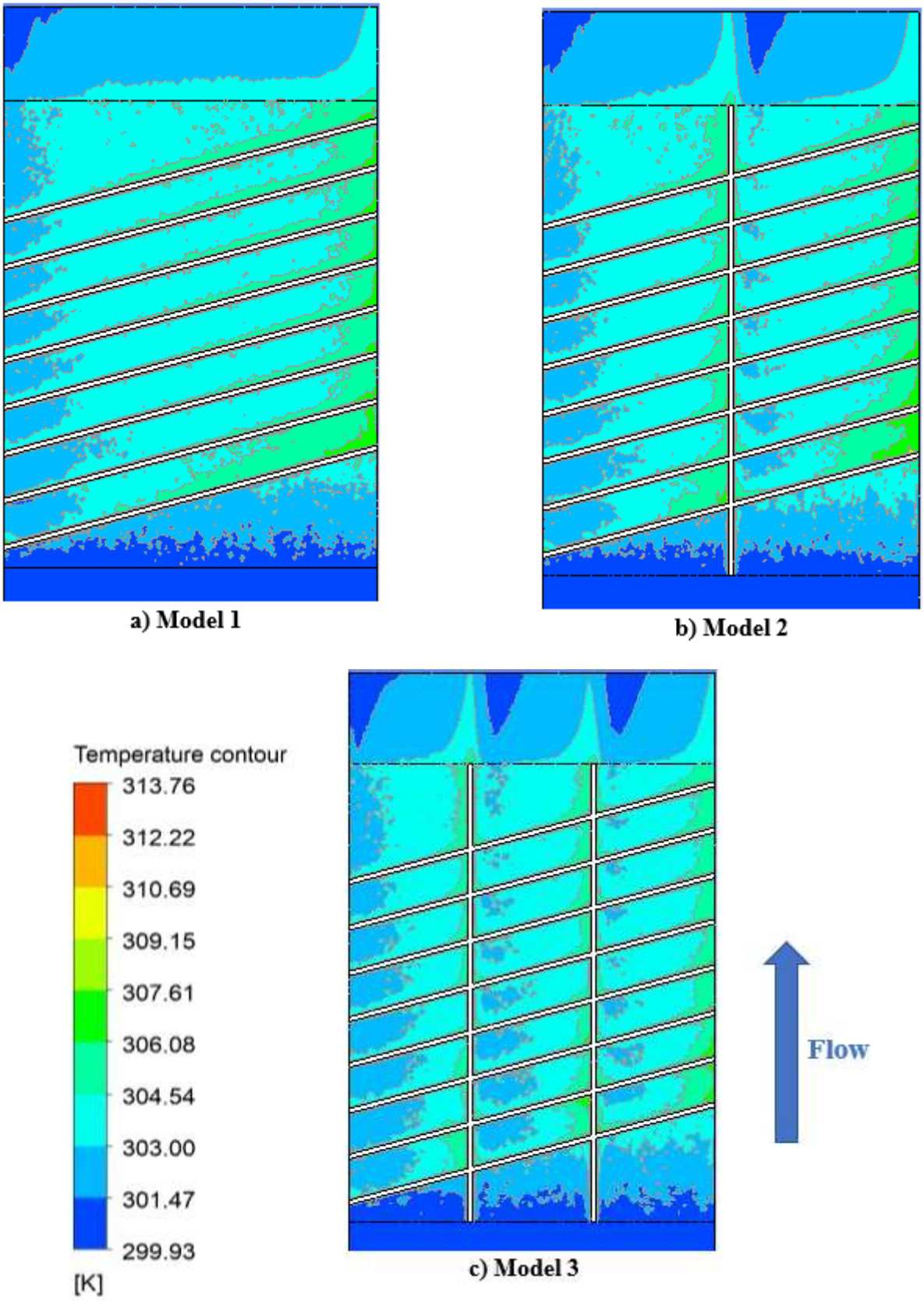


**Figure 11.** Contours of the Fluid Temperature Distribution on the Bottom Surface of Ribbed Models at Re=54,300: a) Model 1; b) Model 2; c) Model 3.

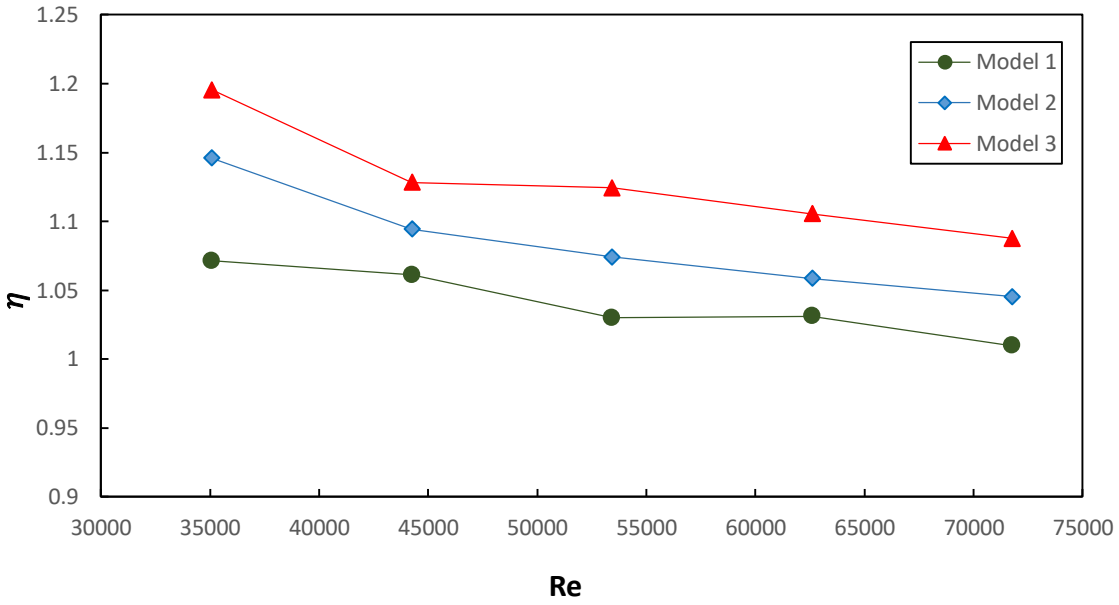


**Figure 12**. Overall Thermal Performance ($\eta$) vs. Reynolds Number for Models 1,2 and 3.

- The decreasing of the heat transfer in the trailing region is increasing with the duct width increase.
- The hybridizing by intersecting ribs with inclined ribs can be considered as an advantageous technique to enhance the heat transfer, rather than using the inclined ribs alone.

## REFERENCES


- AHARWAL, K. R., GANDHI, B. K. & SAINI, J. S. 2008. Experimental investigation on heat-transfer enhancement due to a gap in an inclined continuous rib arrangement in a rectangular duct of solar air heater. *Renewable Energy,* 33**,** 585-596.
- ALFARAWI, S., ABDEL-MONEIM, S. A. & BODALAL, A. 2017. Experimental investigations of heat transfer enhancement from rectangular duct roughened by hybrid ribs. *International Journal of Thermal Sciences,* 118**,** 123-138.
- ALIAGA, D., LAMB, J. & KLEIN, D. 1994. Convection heat transfer distributions over plates with square ribs from infrared thermography measurements. *International journal of heat and mass transfer,* 37**,** 363-374.
- ALKHAMIS, N. Y., RALLABANDI, A. P. & HAN, J.-C. 2011. Heat Transfer and Pressure Drop Correlations for Square Channels With V-Shaped Ribs at High Reynolds Numbers. *Journal of Heat Transfer,* 133**,** 111901-111901-8.
- CHUNG, H., PARK, J. S., PARK, S., CHOI, S. M., RHEE, D.-H. & CHO, H. H. 2015. Augmented heat transfer with intersecting rib in rectangular channels having different aspect ratios. *International Journal of Heat and Mass Transfer,* 88**,** 357-367.

- Fluent 17.1 User's Guide, programing and Tutorial Guide" Fluent, Version 17.1, Ansys Inc, 2018.
- JONES, D. A. & CLARKE, D. B. 2005. Simulation of a wing-body junction experiment using the fluent code. DEFENCE SCIENCE AND TECHNOLOGY ORGANISATION VICTORIA (AUSTRALIA) PLATFORM ….
- KIM, D. H., LEE, B. J., PARK, J. S., KWAK, J. S. & CHUNG, J. T. 2016. Effects of inlet velocity profile on flow and heat transfer in the entrance region of a ribbed channel. *International Journal of Heat and Mass Transfer,* 92**,** 838-849.
- LEE, D. H., RHEE, D.-H., KIM, K. M., CHO, H. H. & MOON, H. K. 2009. Detailed measurement of heat/mass transfer with continuous and multiple V-shaped ribs in rectangular channel. *Energy,* 34**,** 1770-1778.
- LEWIS, M. 1975. Optimising the thermohydraulic performance of rough surfaces. *international Journal of Heat and Mass transfer,* 18**,** 1243-1248.
- LU, B. & JIANG, P.-X. 2006. Experimental and numerical investigation of convection heat transfer in a rectangular channel with angled ribs. *Experimental Thermal and Fluid Science,* 30**,** 513-521.
- MULVANY, N. J., CHEN, L., TU, J. Y. & ANDERSON, B. 2004. Steady-state evaluation of two-equation RANS (reynolds-averaged navier-stokes) turbulence models for high-reynolds number hydrodynamic flow simulations. *Defence Science and Technology Organisation Victoria (Australia) Platform.*
- RAVI, B. V., SINGH, P. & EKKAD, S. V. 2017. Numerical investigation of turbulent flow and heat transfer in two-pass ribbed channels. *International Journal of Thermal Sciences,* 112**,** 31-43.
- TASLIM, M. & LIU, H. 2005. A Combined Numerical and Experimental Study of Heat Transfer in a Roughened Square Channel with 45◦ Ribs. *International Journal of Rotating Machinery,* 2005**,** 60-66.
- YANG, W., XUE, S., HE, Y. & LI, W. 2017. Experimental study on the heat transfer characteristics of high blockage ribs channel. *Experimental Thermal and Fluid Science,* 83**,** 248-259.
- MAHDI, M. M. & GADDOA, A. A. 2019. Outdoor Testing of a Zig-Zag SolarAir heater with and without Artificial Roughness on Absorber Plate. Journal of Engineering, 25, 1-17.
- EZZAT, A. W. & GHASHIM, S. L. 2019. Investigation of Optimum Heat Flux Profile Based on the Boiling Safety Factor. *Journal of Engineering,* 25**,** 139-154.

***Nomenclature***

**Latin Symbols**

| | |
|---|---|
| $D_h$ | Hydraulic diameter of the duct |
| E | Total energy of the fluid which is the sum of internal thermal energy and kinetic energy |
| e | Rib height |
| H | Duct height |
| h | Heat transfer coefficient |
| K | Turbulent kinetic energy or Thermal conductivity |
| L | Length of heated surface |
| P | Pressure |
| p | Rib pitch |
| q | Heat flux |
| T | Temperature |
| u | Velocity |

**Greek Symbols**

| | |
|---|---|
| $\eta$ | Overall thermal performance |
| $\nu$ | Kinematic viscosity |
| $\varepsilon$ | Dissipation Rate of Turbulent Kinetic Energy |
| $\rho$ | Density of air |
| $\omega$ | Specific Dissipation Rate of Turbulent Kinetic Energy |
| $\rho$ | Density of air |
| $\alpha$ | Rib inclination angle |

**Dimensionless Numbers**

| | |
|---|---|
| Nu | Average Nusselt Number = $\frac{h\,D_h}{K_{air}}$ |
| Re | Reynolds number = $\frac{u_m\,D_h}{\nu}$ |
| $e/D_h$ | Relative roughness height |
| p/e | Rib pitch to height ratio |
| f | Friction factor |
| $Nu/Nu_s$ | Nusselt number enhancement ratio |
| $f/f_s$ | Friction factor ratio |

**Subscripts**

| | |
|---|---|
| air | Air |
| b | Bulk Value |
| c | Cross-Section |
| cond | Heat transferred by conduction |
| conv | Heat transferred by forced convection |
| in | Inlet |
| m | Mean |
| out | Outlet |
| s | Test surface (smooth surface) |
| x,y,z | Cartesian Coordinate |